EUROPEAN MECHANICAL SCIENCE

Research Article

e-ISSN: 2587-1110

Effect of prior deformation on microstructural evolution and retained austenite stability in bainite–martensite structures of continuously cooled low-carbon steel

Emre Alan[1*]

[1]ÇEMTAŞ Çelik Mak. San. ve Tic. A. Ş., R&D Center, Bursa, Türkiye

Abstract: This study investigates the effects of prior deformation and continuous cooling rate on microstructural evolution and retained austenite stability in a low-carbon steel containing 0.15–0.20 wt.% carbon. Continuous cooling was applied to laboratory-scale specimens at cooling rates of 1–8 °C/s under both deformed (strain: 0.55, at 1200 °C) and undeformed conditions. Optical microscopy, scanning electron microscopy, and X-ray diffraction techniques were used for microstructural quantification. The results demonstrated that under undeformed conditions, increasing the cooling rate led to a progressive transformation from bainite to martensite. A transition from 86.5% bainite and 13.5% martensite at 1 °C/s to a fully martensitic structure at 8 °C/s was observed, corresponding to an increase in average hardness from 326 HV to 505 HV. Deformation in austenite region significantly accelerated transformation kinetics, as evidenced by a leftward shift in the deformation-modified continuous cooling transformation diagram. The deformed specimen cooled at 4 °C/s exhibited nearly similar microstructure (70.5% bainite, 29.5% martensite) and hardness ($379^{\pm 10}$ HV) with the undeformed specimen cooled at 2 °C/s ($361^{\pm 12}$ HV). In undeformed conditions, retained austenite volume fraction increased up to 13.9% with cooling rate. However, deformation prior to cooling substantially reduced retained austenite content (7.9% at 4 °C/s), despite identical thermal histories. The findings highlight the importance of controlling both deformation and cooling on tailoring final microstructures and mechanical properties without the need for additional heat-treatments. The results provide an insight into optimizing energy-efficient and low-emission forging processes aimed at improving uniformity in components with varying cross-sections.

Keywords: Steel; continuous cooling; microstructure; phase transformation; retained austenite.

1. Introduction

Steel production is one of the most energy-intensive industrial sectors, accounting for approximately 8% of total global CO_2 emissions [1]. In addition to decarbonization efforts in primary steelmaking, considerable potential opportunities exist in optimizing downstream thermo-mechanical processing routes like hot forging for lowering energy requirements and process emissions [2–5]. Traditionally, forged steel components, especially in the automotive industry, undergo a subsequent quenching and tempering (Q&T) heat treatment after hot forging to attain high strength in combination with adequate toughness. However, the elevated processing temperatures and extended Q&T heat treatment durations significantly increase both energy consumption and CO_2 emissions. To address these challenges, the development of energy-efficient and low-emission forging strategies, which eliminate or minimize post-forging heat treatments, has become increasingly important for industrial applications. A promising approach involves tailoring the microstructure directly during hot forging through controlled deformation and continuous cooling, thereby reducing energy consumption and environmental impact [6,7]. Successful implementations of both newly developed continuously cooled steels and tailored continuous cooling strategies to achieve high mechanical performance have been reported in the literature [8 - 10].

In the continuous cooling process, the selection of alloying elements and the cooling rate are critical pa-

*Corresponding author:
Email: emre48@gmail.com

Cite this article as:
Alan, E. (2025). Effect of prior deformation on microstructural evolution and retained austenite stability in bainite–martensite structures of continuously cooled low-carbon steel. *European Mechanical Science*, 9(3): 291-301. https://doi.org/10.26701/ems.1726120

History dates:
Received: 24.06.2025, *Revision Request*: 27.07.2025, *Last Revision Received*: 29.07.2025, *Accepted*: 18.08.2025

rameters that determine the final microstructure and, consequently, the mechanical properties of steel. However, these modifications also increase raw material and processing costs. As noted by Gramlich et al. [3], developing steel grades that balance performance with cost and environmental impact remains a central challenge in sustainable materials design. Nevertheless, when the process and operational costs of Q&T heat treatment are taken into account, the cumulative cost of enhanced alloying can offer a more cost-effective and sustainable strategy in hot forging process routes [6]. Even within narrow composition limits, variations in carbon, manganese, chromium and molybdenum contents in steel significantly influence transformation behavior and mechanical properties. It was reported that increases in carbon by 0.01 wt.% can raise hardness by ~30 HV, while additions of manganese (~1.8–2.5 wt.%) and molybdenum (~0.1–0.2 wt.%) enhance bainite formation and retained austenite (RA) stability depending on continuous cooling conditions [7]. Therefore, the influence of chemical composition should be evaluated alongside with cooling rate to effectively design forging routes that achieve improved microstructural characteristics. Mandal et al. [8] reported that increasing the continuous cooling rate from 1 to 10 °C/s in a low-carbon bainitic steel with 0.2 wt.% carbon resulted in a microstructural transition from lower bainite to fully martensitic structures, accompanied by a hardness increase from 290 HV to over 500 HV. Kim et al. [14] achieved a fine balance of martensite and thin-film RA in low carbon steel with 2.0 wt.% manganese content using double-step continuous cooling, yielding RA contents of approximately 15% and tensile strengths exceeding 1200 MPa.

The cooling rate is primarily influenced by the cooling medium and the cross-sectional dimensions of the cooled steel component. During hot forging, plastic deformation inherently alters the local thickness of the forged sections, thereby modifying local cooling rates. In addition to thickness variations, parameters such as deformation temperature and strain influence the austenite transformation kinetics and the resulting microstructure.

Previous studies have shown that deformation causes a shift in continuous cooling transformation (CCT) diagrams, accelerating the austenite transformation by promoting shorter transformation times and higher transformation temperatures. For instance, Kawulok et al. [11] investigated the deformation behavior of continuously cooled 20MnCr5 and 32CrB4 steels and reported that plastic deformation significantly accelerates phase transformations compared to undeformed conditions. Similar observations have been made in low-carbon and medium-carbon TRIP-assisted steels, where deformation causes a notable leftward shift in the transformation curves [12].

Furthermore, both deformation and cooling rate affect the volume fraction and morphology of RA in the final microstructure. In medium-carbon steels, an increased cooling rate has been associated with higher RA content [13], whereas higher deformation ratios tend to reduce RA content [14]. It has also been suggested that when RA forms in a thin-film morphology, it remains mechanically stable and contributes positively to the overall mechanical performance [15].

Hot-forged steels are typically used in applications where high mechanical performance and reliability are required [16, 17]. Therefore, achieving uniform microstructure and mechanical properties throughout the entire cross-section of forged components is crucial. However, the inherently non-uniform geometry of forged parts often results in variable cross-sectional thicknesses, leading to heterogeneous deformation and cooling conditions. As a result, careful design of deformation and cooling parameters is essential to ensure microstructural consistency across the component.

This study investigates the synergistic effects of hot deformation and continuous cooling rate on the microstructural evolution of forged steel. Unlike previous studies, continuous cooling transformation diagrams were developed under both static and dynamic conditions to assess the feasibility of achieving uniform microstructures across sections with varying deformation ratios. It is anticipated that the methodology proposed in this work will facilitate the design of forging processes that ensure homogeneity in final properties, thereby contributing to both performance optimization and environmental sustainability.

2. Material and Methods

Hot forging operations are typically conducted on round-sectioned, hot-rolled steel raw materials. In the present study, laboratory-scaled raw materials were produced in a process route comparable to industrial practice, involving melting, alloying, casting, and hot rolling processes. A schematic representation of laboratory-scale production is given in ▶**Figure 1**.

The melting and casting stages were carried out in a 50-kW induction furnace with a capacity of 15 kg liquid steel. In order to prevent re-oxidation of liquid steel, both processes were conducted under vacuum atmosphere. The molten steel was poured into a permanent mold by using gravity casting method. Following solidification, billets with a round cross-section of Ø70 mm were obtained. The chemical composition of the steel was analyzed by optical emission spectrometry (OES) is presented in ▶**Table 1**.

Prior to hot deformation process, the billets were reheated to 1150 °C. Hot deformation process was applied by using a laboratory-scale hot rolling physical simulator. After six roll passes with approximately 25% deformation was applied at each pass, hot-rolled bars with a final diameter of Ø30 mm were produced.

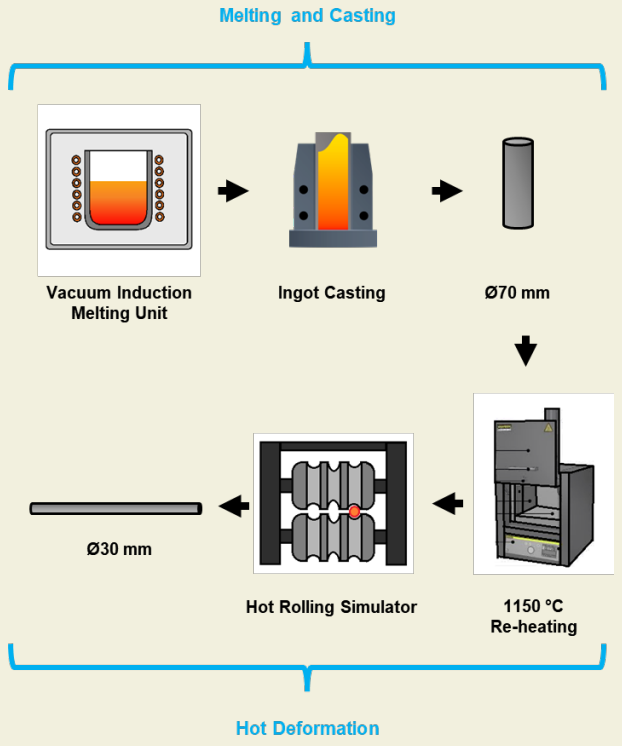

Figure 1. A schematic view of the laboratory-scale production route.

Hot-forging simulations and continuous cooling experiments were performed with a Gleeble 3800 thermo-mechanical simulator. Cylindrical specimens with a diameter of 10 mm and a length of 15 mm were prepared from previously hot-rolled steel bars. The specimens were heated to 1200 °C at a rate of 5 °C/s and held for 20 s to ensure complete austenitization. Then, the specimens were either deformed or left undeformed before cooling to 1040 °C. Continuous cooling was subsequently applied at cooling rates of 1 °C/s, 2 °C/s, 4 °C/s, and 8 °C/s. A schematic representation of the hot-forging and cooling procedures, along with the associated process parameters, is provided in ▶**Figure 2**.

Table 1. Chemical composition of the produced steel [wt.%].

	C	Si	Mn + Cr	Mo	Ti	Nb	B
Min.	0.15	0.15	2.10	0.10	0.0100	0.0250	0.0010
Max.	0.20	0.35	2.55	0.20	0.0400	0.0500	0.0040

Microstructural characterization was conducted using optical microscopy (OM) and scanning electron microscope (SEM). Following standard metallographic preparation, the specimens were etched with Le Pera solution to differentiate microstructural constituents. In Le Pera etching, martensite appears dark beige/straw colored regions while bainite exhibits bluish [36]. The area fractions of each microstructure were quantified via color-based image analysis using software ImageJ. For each cooling conditions, four different OM images at 100X magnification were analyzed and the average microstructural content was determined and assigned to the corresponding cooling rate.

Vickers microhardness measurements were performed using an Emco-Test DuraScan hardness tester under two different loads, each applied with a dwelling time of 5 s. A 0.1 kgf load was employed to measure the hardness of individual microstructural constituents, whereas a 0.3 kgf load was used to determine the average hardness of the specimens. Five separate measurements were taken from each specimen.

The retained austenite (RA) contents of specimens were quantified using X-ray diffraction (XRD) with a Cu-Kα cathode tube. Scans were conducted over a 2θ range of 30° to 100° at a scanning speed of 0.5 °/s. The volume fractions of RA were calculated via Rietveld refinement method using MAUD software. Additionally, electron backscatter diffraction (EBSD) analysis was employed to provide more detailed insights into the morphology

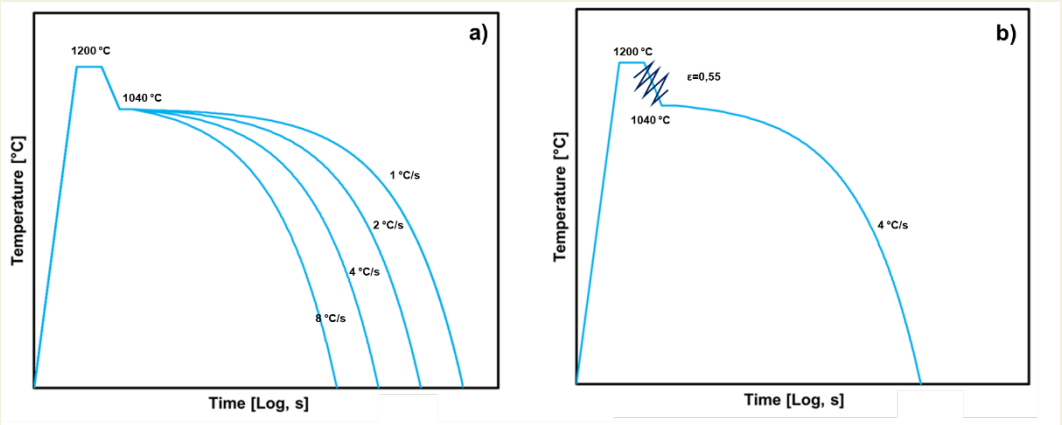

Figure 2. A schematic view of the heating, hot deformation and cooling processes of **(a)** undeformed, **(b)** deformed specimens.

and distribution of RA in both deformed and undeformed specimens cooled at 4 °C/s.

3. Results and Discussion

3.1. Effect of Cooling Rate on Microstructural Evolution

In this section, the influence of cooling rate on microstructure was investigated under undeformed conditions. During heating, dimensional changes observed in the dilatometric curves corresponded to the onset of austenite formation (A_{e1}) and the completion of the austenitization process (A_{c3}). Upon cooling, the shape and slope of the dilatometric curves vary notably for the same steel, reflecting differences in transformation mechanisms and kinetics. At relatively slower cooling rates, a gradual and continuous change in specimen length may observed during cooling, indicating the occurrence of transformation products such as ferrite and bainite. Ferrite forms via a diffusional mechanism at higher temperatures, while bainite forms at intermediate temperatures through a shear-assisted transformation mechanism that involves limited diffusion of carbon. The bainite transformation is governed by displacive nucleation and carbon partitioning, resulting in the formation of bainitic ferrite along with retained austenite or carbides, depending on cooling conditions and chemical composition [30 – 32]. In contrast, at higher cooling rates, the curves exhibit sharper and more abrupt contractions as a characteristic of martensitic transformation. Martensite forms via a diffusionless shear mechanism once Ms temperature is reached, leading to a sudden volumetric contraction and a distinct change in the slope of the curve [33, 34].

The dilatation curves of specimens during continuous cooling are given in ▶**Figure 3**. At lower cooling rates, the curves exhibit smooth and gradual contractions over a broad temperature range, with transformation events initiating around 500 °C which indicatives of bainitic transformation. As the cooling rate increases, the transformation region shifts to lower temperatures as consistent with martensitic transformation. The observed progression from gradual to sharp curve features with increasing cooling rate reflects the suppression of bainite and the growing dominance of martensite, in line with common transformation behavior in low-carbon steels [31, 33].

The static CCT diagram of the steel used in this study is shown in ▶**Figure 4**. A fully martensitic microstructure was obtained at a cooling rate of 8 °C/s, while mixed bainitic–martensitic microstructures were observed at intermediate cooling rates between 1 and 4 °C/s. The results show good agreement with CCT diagrams reported in the literature for low-carbon steels with similar carbon and microalloying additions [35].

▶**Figure 5** shows OM images of undeformed specimens subjected to continuously cooled at rates of 1 °C/s, 2 °C/s,

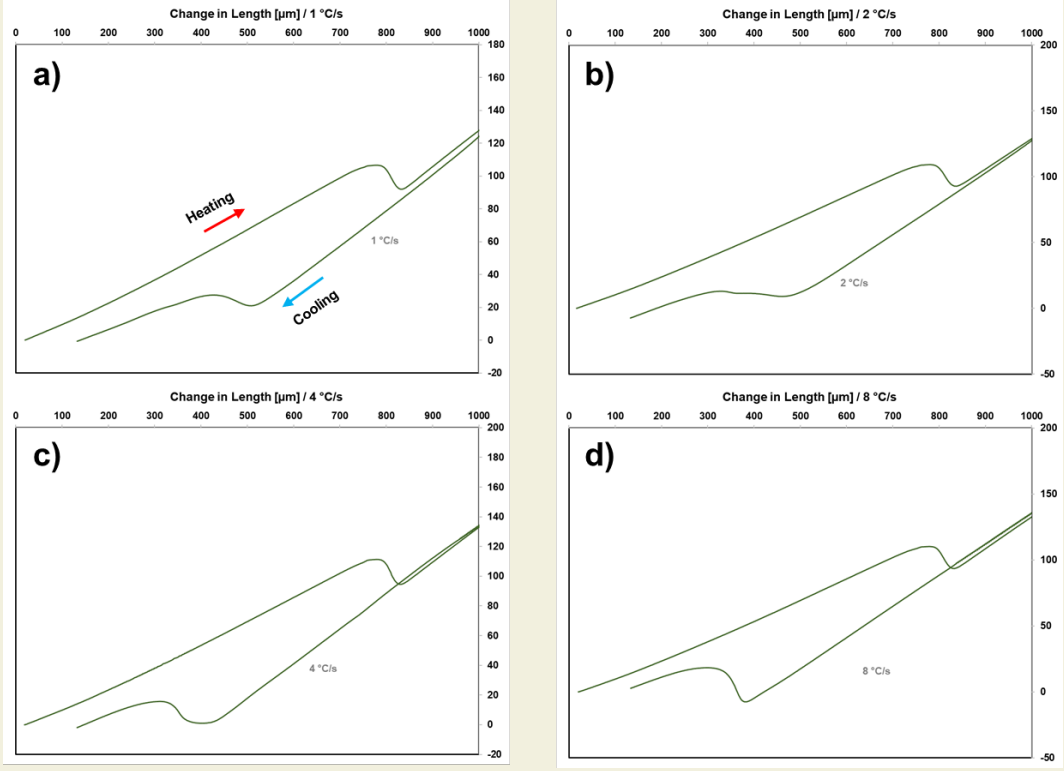

Figure 3. Dilatometric curves of specimens during continuous cooling with different cooling rates **(a)** 1 °C/s, **(b)** 2 °C/s, **(c)** 4 °C/s and **(d)** 8 °C/s.

4 °C/s and 8 °C/s. At the lowest cooling rate of 1 °C/s, the microstructure primarily consists of bainite, visible as bluish regions accompanied by a relatively small fraction of martensite. As the cooling rate increases to 2 °C/s and 4 °C/s, the fraction of martensite gradually increases, indicating a transition from a mainly bainitic to a mixed bainite–martensite microstructure. At the highest cooling rate of 8 °C/s the microstructure is almost fully martensitic with no observable bainite. This transformation trend is consistent with the static CCT diagram of the steel, wherein the transformation path intersects the bainitic region before reaching the martensite start temperature at slower cooling rates, thereby allowing sufficient time for bainite formation. In contrast, at higher cooling rates, the transformation path bypasses or only briefly intersects the bainitic region, suppressing bainite formation and favoring a predominantly martensitic transformation.

▶**Figure 6** presents SEM micrographs of undeformed specimens subjected to continuously cooled at rates of 1, 2, 4, and 8 °C/s. The evolution of microstructure with increasing cooling rate is consistent with the transformation paths predicted by the static CCT diagram of steel. At the lowest cooling rate of 1 °C/s, the microstructure is dominated by bainite. Due to the slower cooling rate, the morphology of bainite mostly formed as granular shape as expected. At 2 °C/s and 4 °C/s cooling rates, a more balanced mixture of bainite and martensite is observed. However, lower bainite morphology takes part as the cooling rate increases while martensite appears as lath structures.

The quantitative microstructural analysis and microhardness measurements of continuously cooled undeformed specimens are presented in ▶**Figure 7**. At the lowest cooling rate of 1 °C/s, the microstructure consists of approximately 86.5% bainite and 13.5% martensite. As the cooling rate increases, a clear transition in microstructure from predominantly bainitic to fully martensitic is observed. The calculated area fractions of each microstructural constituents align with the OM and SEM images where slower cooling rates allow sufficient time for bainite formation whereas faster cooling suppresses bainitic transformation and promotes martensite formation. The corresponding microhardness data also reflects the microstructural evolution. Bainite exhibits lower hardness values, ranging from approximately 289 to 371 $HV_{0.1}$, whereas martensite displays significantly higher hardness values over 500 $HV_{0.1}$.

The result of microhardness measurements of undeformed specimens conducted under 0.3 kgf load is given in ▶**Figure 8**. The overall hardness of the steel increases with cooling rate, primarily due to the increasing fraction of martensite. A marked rise in hardness is observed beyond a cooling rate of 2 °C/s, which corresponds to the onset of martensite dominance in the microstructure. This trend underscores the significant influence of martensitic transformation on the mechan-

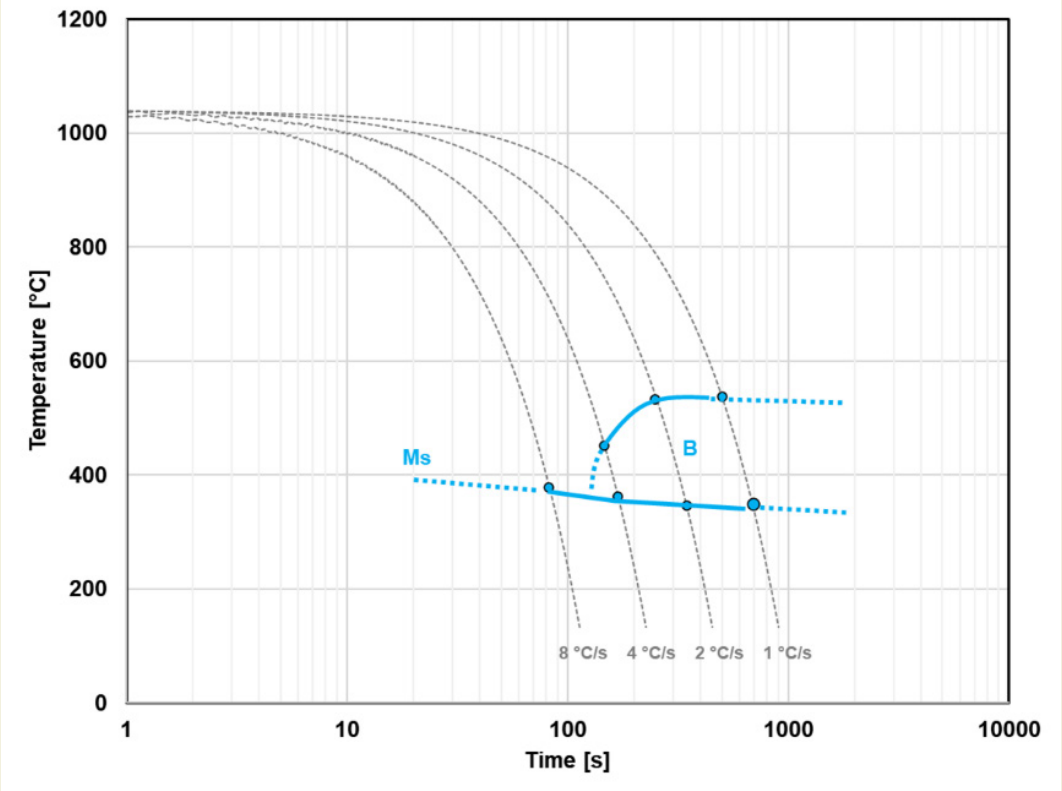

Figure 4. CCT diagram of experimental steel.

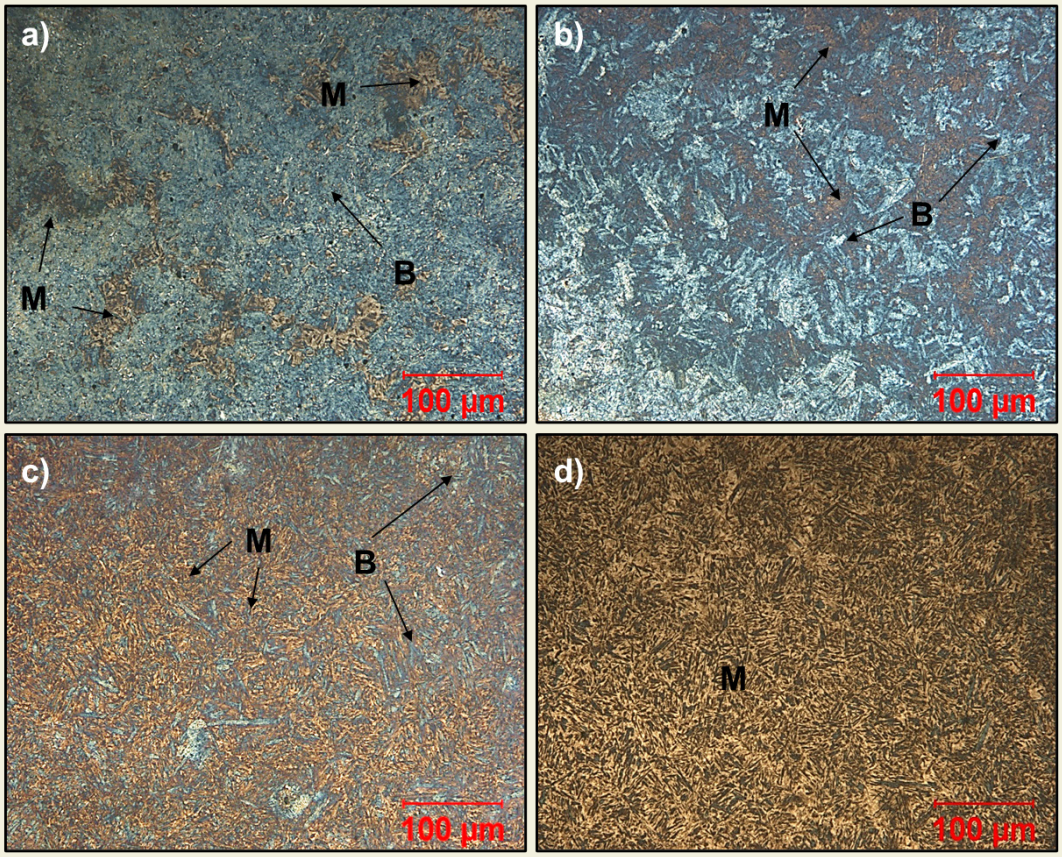

Figure 5. OM images of the undeformed specimen cooled at 1 **(a)** 1 °C/s, **(b)** 2 °C/s, **(c)** 4°C/s and **(d)** 8 °C/s.

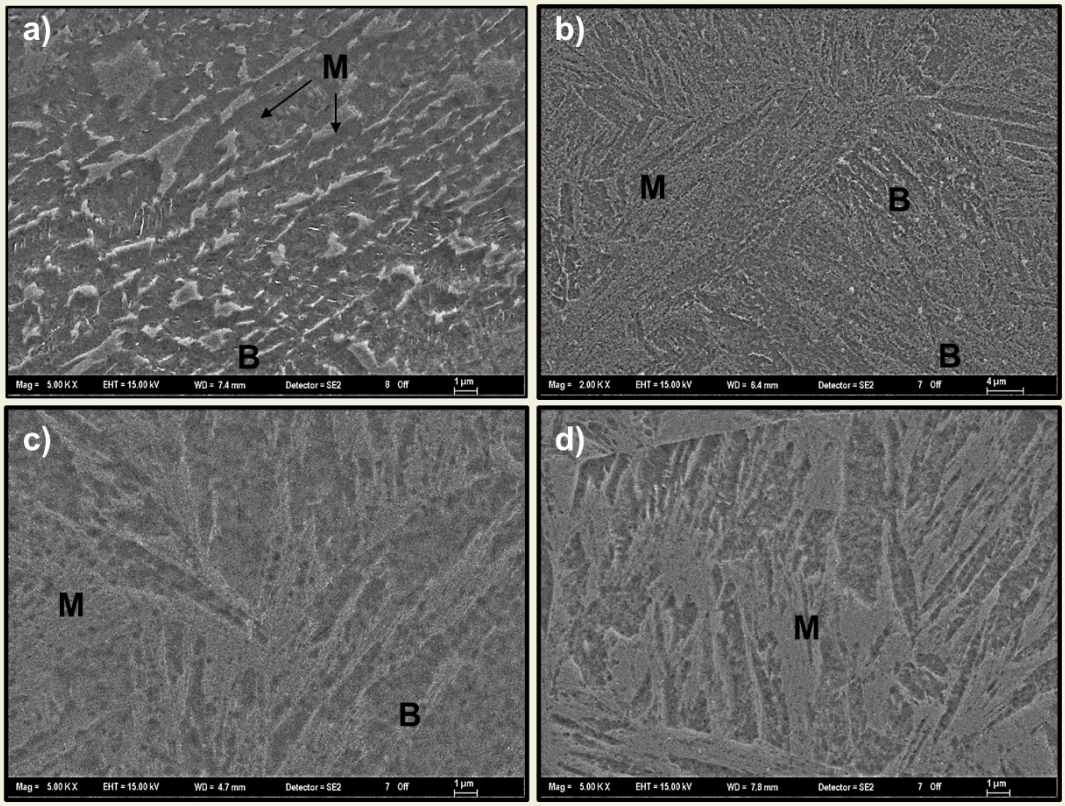

Figure 6. SEM images of the undeformed specimen cooled at 1 **(a)** 1 °C/s, **(b)** 2 °C/s, **(c)** 4°C/s and **(d)** 8 °C/s.

ical response of the steel.

3.2. Effect of Deformation on Microstructural Evolution

▶**Figure 9** shows OM and SEM micrographs of the specimen subjected to plastic deformation at a strain level of 0.55 and subsequently cooled at a rate of 4 °C/s. The resulting microstructure predominantly consists of bainitic ferrite with both coarse and fine morphologies, forming a bainite–martensite mixed structure. The area fractions of bainite and martensite were calculated as 70.5% and 29.5%, respectively. Microhardness measurements of the bainitic regions ranged between 326 and 359 $HV_{0.1}$, while martensitic regions exhibited higher values ranging from 454 to 510 $HV_{0.1}$. The average microhardness measured under 0.3 kgf load was found to be 379 HV.

As shown in ▶**Figure 10**, at a strain level of 0.55, the deformed specimen that cooled at 4 °C/s exhibited a microstructural composition and hardness distribution remarkably similar to those of the undeformed specimen cooled at 2 °C/s. This suggests that prior plastic deformation significantly accelerates bainite transformations during continuous cooling. The microstructural characteristics and mechanical response observed in the deformed specimen under 4 °C/s cooling are nearly equivalent to those of the undeformed specimen at a slower cooling rate, corroborating the transformation kinetics shift introduced by deformation.

▶**Figure 11** compares the conventional CCT diagram with the deformation-modified (D-CCT) transformation curves, highlighting the leftward shift in bainitic transformation start times caused by prior plastic deformation. This mechanism can be attributed to several metallurgical factors. Plastic deformation within the austenite temperature range introduces a high density of dislocations and defects, which act as heterogeneous nucleation sites for bainitic ferrite. This increased nucleation site density accelerates the transformation kinetics, effectively shifting the bainitic start to shorter times and higher temperatures [37, 38]. Moreover, deformation promotes a refinement of the prior austenite grain structure, further facilitating bainite formation at earlier stages of cooling [39]. Additionally, the start temperature of martensitic transformation (Ms) was

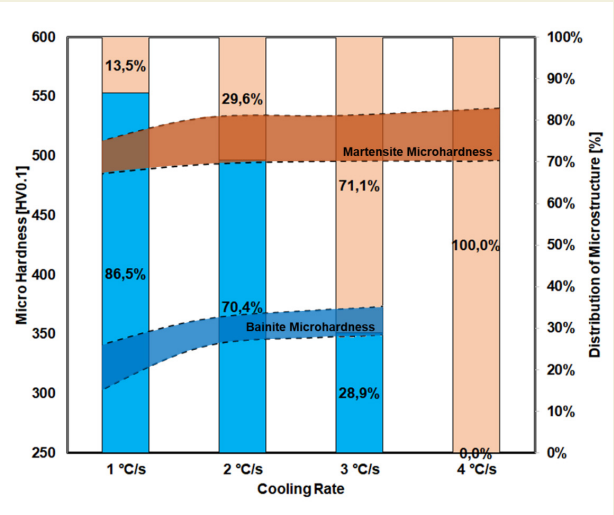

Figure 7. Microstructure fractions and corresponding microhardness [$HV_{0.1}$] values of bainite and martensite in undeformed specimens.

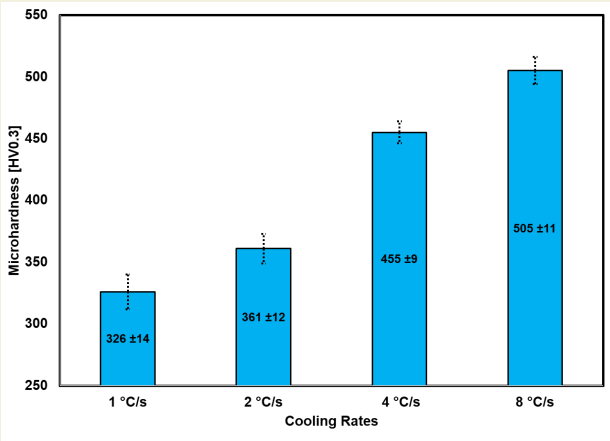

Figure 8. Microhardness [HV0.3] measurements of undeformed specimens.

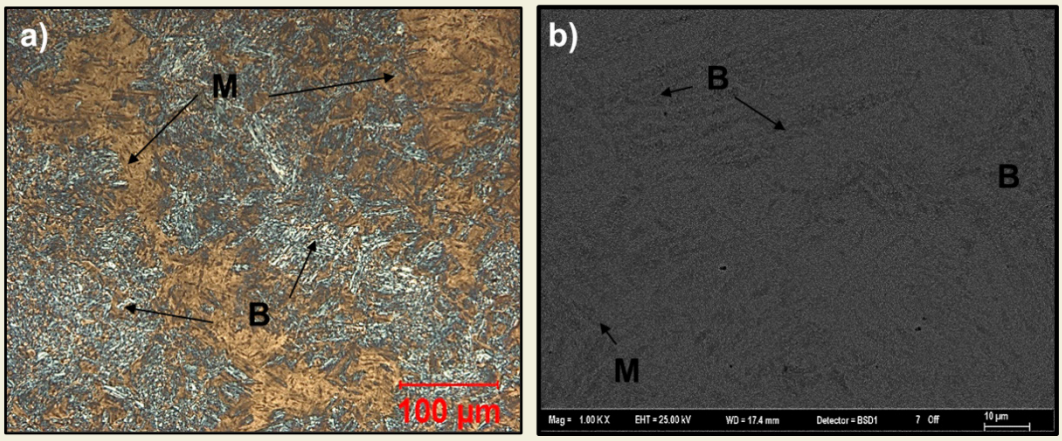

Figure 9. OM and SEM micrographs of the deformed specimen cooled at 4 °C/s; **(a)** OM, **(b)** SEM.

https://doi.org/10.26701/ems.1726120

found to be more strongly influenced by the cooling rate than by prior deformation. Specifically, higher cooling rates resulted in increased Ms temperatures, whereas lower cooling rates led to a decrease. This trend suggests that the thermal history exerts a dominant influence on martensitic transformation onset, regardless of the deformation history in the austenitic phase.

3.3. Retained Austenite (RA)

RA is a metastable phase that can transform into martensite under the influence of stress or temperature changes. This transformation mechanism, known as Transformation-Induced Plasticity (TRIP), may lead to unpredicted variations in mechanical properties. The stability of RA in steels depends on several factors including internal or external stress states, chemical composition: particularly carbon and manganese content, prior austenite grain boundaries (PAGBs), RA morphology, and the characteristics of the surrounding microstructures [20 - 24].

▶**Figure 12** shows the volume fractions of retained austenite measured in both deformed and undeformed specimens. In undeformed conditions, increasing the cooling rate led to a higher RA content. However, in specimens deformed prior to cooling at 4 °C/s, the RA content was significantly reduced compared to their undeformed counterparts. Previous studies have attributed this phenomenon to the instability of RA formed under mechanical or chemical conditions that are unfavorable to its retention, particularly following post-transformation deformation [25 - 27]. However, in the present study, deformation was applied within the austenite temperature region, prior to microstructural transformation temperatures on cooling. It was seen that pre-transformation deformation shifted the transformation kinetics, promoting the earlier formation of high-temperature microstructures compared to undeformed conditions. RA is expected to form within or between bainitic ferrite laths during cooling. Despite the higher cooling rate, bainitic laths in deformed samples were observed to be coarser than those in undeformed specimens, suggesting a change in RA morphology from lath like to blocky regions. As reported in earlier studies, such blocky morphologies of RA are mechanically unstable and prone to transformation into martensite even during sample preparation for microstructural analysis [28, 29].

▶**Figure 13** presents EBSD phase maps comparing the retained austenite content in deformed and undeformed samples cooled at 4 °C/s. The RA content was measured as 7.9% in the deformed specimen while undeformed specimen resulted 13.9%. These values align well with the XRD measurements, although EBSD consistently yielded slightly lower results. This discrepancy is attributed to the limited spatial resolution and penetration depth of EBSD compared to bulk-sensitive techniques such as XRD. Due to its surface sensitivity and smaller sampling volume, it is thought that EBSD may tend to underestimate the total RA content.

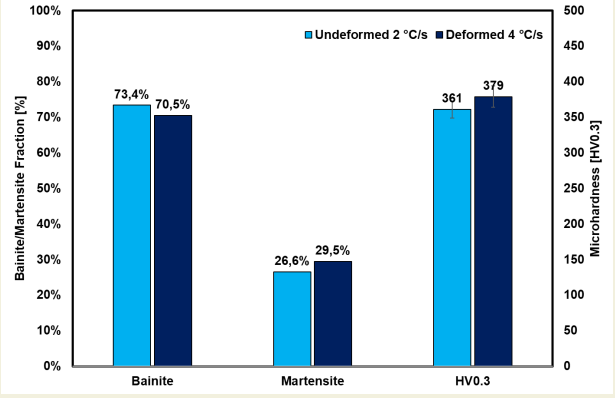

Figure 10. Area fractions and microhardness [HV0.3] values of undeformed specimen cooled at 2 °C/s and deformed specimen cooled at 4 °C/s.

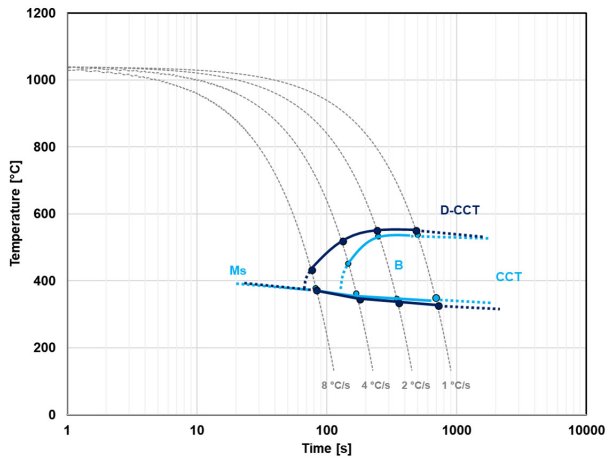

Figure 11. Comparison between conventional CCT and deformation-modified CCT (D-CCT) diagrams showing the shift in transformation onset on account of prior plastic deformation.

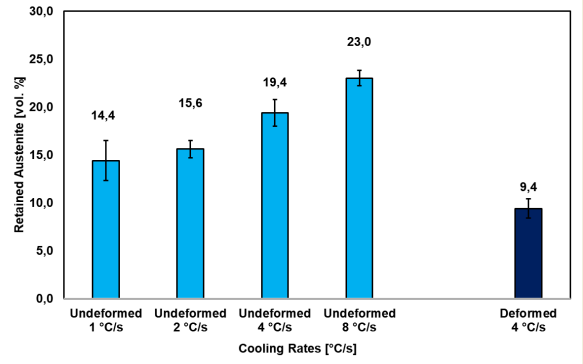

Figure 12. Volume fractions of retained austenite in deformed and undeformed specimens (XRD measurements).

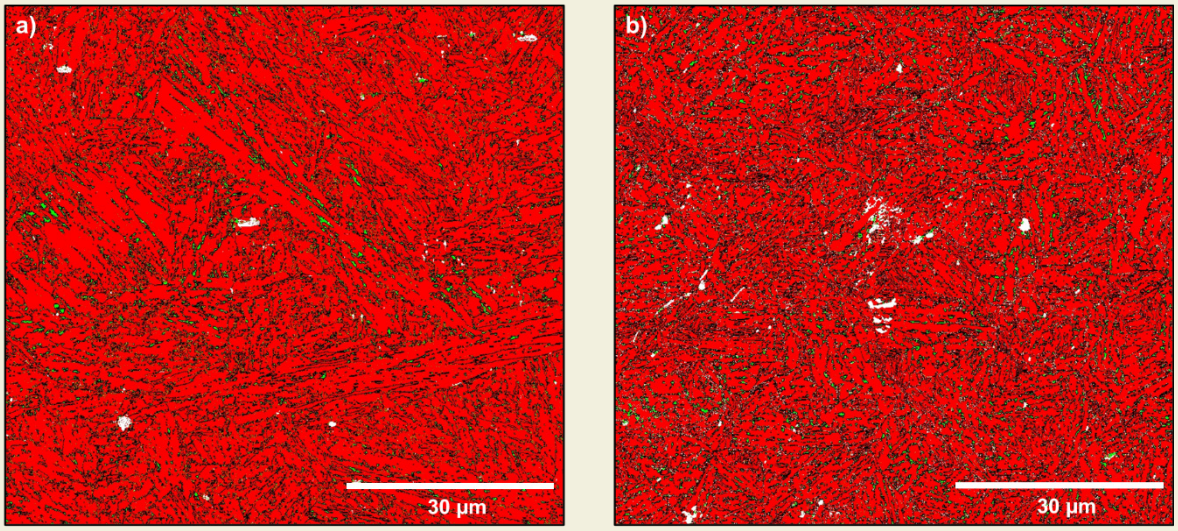

Figure 13. EBSD phase maps comparing retained austenite distribution in **(a)** deformed and **(b)** undeformed specimens cooled at 4 °C/s.

4. Conclusions

In this study, the combined effects of hot deformation and continuous cooling rate on the microstructural evolution of hot-forged low-carbon steel were systematically investigated. Based on the experimental findings, the following conclusions can be drawn:

- In continuous cooling, under undeformed conditions, the resulting microstructure was highly sensitive to the applied cooling rate.
- Increasing the cooling rate progressively shifted the microstructure from bainitic to martensitic. At a cooling rate of 8 °C/s, a fully martensitic structure was obtained, whereas lower rates produced mixed bainitic–martensitic microstructures.
- Pre-transformation deformation significantly accelerated transformation kinetics of bainite as evidenced by the leftward shift in the deformation-modified continuous cooling transformation diagram relative to the conventional CCT diagram. For a strain level of 0.55, the deformed sample cooled at 4 °C/s exhibited highly comparable microstructural and hardness characteristics to the undeformed sample cooled at 2 °C/s.
- The martensitic transformation was found to be more strongly influenced by the cooling rate than by prior deformation.
- The RA content increased with cooling rate in undeformed conditions. However, deformation prior to cooling substantially reduced RA content at identical cooling rates. This reduction is attributed to the formation of mechanically unstable blocky RA morphologies within coarser bainitic structures induced by deformation.

In summary, this study demonstrates that microstructural and mechanical properties of hot-forged steels can be effectively tailored by controlling deformation parameters and cooling rates. These findings offer a scientific foundation for designing energy-efficient, low-emission forging routes capable of producing mechanically homogeneous components without the need for additional heat treatments.

Acknowledgments

This research was supported by The Scientific and Technological Research Council of Turkey (TUBITAK) 1002-A Programme under the application number of 222M041

Research ethics

Not applicable.

Artificial Intelligence Use

The author(s) declare that no generative artificial intelligence (e.g., ChatGPT, Gemini, Copilot, etc.) was used in any part of this study.

Author contributions

The author solely conducted all stages of this research.

The author has accepted responsibility for the entire content of this manuscript and approved its submission.

Competing interests

The author states no conflict of interest.

Research funding

This research was supported by The Scientific and Technological Research Council of Turkey (TUBITAK) 1002-A Programme under the application number of 222M041.

Data availability

Not applicable.

Peer-review

Externally peer-reviewed.

Orcid

Emre Alan https://orcid.org/0000-0002-1894-0231

5. References

[1] Raabe, D., Matic Jovičević-Klug, Ponge, D., Gramlich, A., Silva, Grundy, A. N., Springer, H., Filho, I. S., & Ma, Y. (2024). Circular Steel for Fast Decarbonization: Thermodynamics, Kinetics, and Microstructure Behind Upcycling Scrap into High-Performance Sheet Steel. Annual Review of Materials Research, 54(1), 247–297. https://doi.org/10.1146/annurev-matsci-080222-123648

[2] Kumar, R. S., Kumar, T. P., Daniel, S., Gugapriyan, R., & Shamanth, S. (2024). A review on sustainable manufacturing through green techniques. AIP Conference Proceedings, 3232, 020014. https://doi.org/10.1063/5.0235892

[3] Gramlich, A., Helbig, C., Schmidt, M., & Hagedorn, W. (2024). A comprehensive design approach to increase the performance of steels under minimal costs and environmental impacts. Sustainable Materials and Technologies, 41, e01040–e01040. https://doi.org/10.1016/j.susmat.2024.e01040

[4] Sun, C., Wang, J., Zhou, M., Hong, L., Ai, L., & Wen, L. (2024). Process Path for Reducing Carbon Emissions from Steel Industry—Combined Electrification and Hydrogen Reduction. Processes, 12(1), 108–108. https://doi.org/10.3390/pr12010108

[5] Holappa, L. (2020). A General Vision for Reduction of Energy Consumption and CO2 Emissions from the Steel Industry. Metals, 10(9), 1117. https://doi.org/10.3390/met10091117

[6] Hagedorn, W., Gramlich, A., Greiff, K., & Krupp, U. (2022). Alloy and process design of forging steels for better environmental performance. Sustainable Materials and Technologies, 34, e00509–e00509. https://doi.org/10.1016/j.susmat.2022.e00509

[7] Alan, E., Ayhan, İ. İ., Ögel, B., & Uzunsoy, D. (2024). A comparative assessment of artificial neural network and regression models to predict mechanical properties of continuously cooled low carbon steels: an external data analysis approach. Journal of Innovative Engineering and Natural Science, 4(2), 495–513. https://doi.org/10.61112/jiens.1445518

[8] Mandal, G., Dey, I., Mukherjee, S., & Ghosh, S. K. (2022). Phase transformation and mechanical properties of ultrahigh strength steels under continuous cooling conditions. Journal of Materials Research and Technology, 19, 628–642. https://doi.org/10.1016/j.jmrt.2022.05.033

[9] Gramlich, A., T. Schmiedl, S. Schönborn, Melz, T., & Bleck, W. (2020). Development of air-hardening martensitic forging steels. Materials Science and Engineering A, 784, 139321–139321. https://doi.org/10.1016/j.msea.2020.139321

[10] Furkan Yılmaz Küçükakarsu, İsmail İrfan Ayhan, Alan, E., Demet Taştemür, & Süleyman Gündüz. (2022). Effect of hot rolling process parameters on the microstructure and mechanical properties of continuously cooled low-carbon high-strength low-alloy (HSLA) steel. Materials Testing, 64(8), 1136–1149. https://doi.org/10.1515/mt-2021-2220

[11] Kawulok, R., Schindler, I., Kawulok, P., Rusz, S., Opěla, P., Kliber, J., Solowski, Z., Čmiel, K. M., Podolínský, P., Mališ, M. & Vašek, Z. (2016). Transformation kinetics of selected steel grades after plastic Deformation, Metalurgija, 55(3), pp.357-360. https://doi.org/10.13140/RG.2.1.1401.0001

[12] Grajcar, A., & Opiela, M. (2008). Influence of plastic deformation on CCT- diagrams of low-carbon and medium- carbon TRIP-steels Manufacturing and processing. Journal of Achievements in Materials and Manufacturing Engineering A.

[13] Abdulkareem, N. M. & Jabbar, M. A. (2017). Effect of Retained Austenite on the Micro-structure and Mechanical Properties of Al-Si4340 High Strength Low Alloy Steel (HSLA steel) Using Magnetic Saturation Measurement and x-ray Diffraction methods, Basrah Journal for Engineering Sciences, 17(2). https://doi.org/0.33971/bjes.17.2.1

[14] Kim, K.-W., Kim, K. I., Lee, C.-H., Kang, J.-Y., Lee, T.-H., Cho, K.-M., & Oh, K. H. (2016). Control of retained austenite morphology through double bainitic transformation. Materials Science and Engineering A, 673, 557–561. https://doi.org/10.1016/j.msea.2016.07.083

[15] Garcia-Mateo, C., & Caballero, F. G. (2005). The role of retained austenite on tensile properties of steels with bainitic microstructures. Materials Transactions, 46(8), 1839–1846. https://doi.org/10.2320/matertrans.46.1839

[16] Kang, M., Park, M., Kim, B., Kim, H. C., Jeon, J. B., Kim, H., … Kim, B. J. (2021). Effect of Heat Treatment on Microstructure and Mechanical Properties of High-Strength Steel for in Hot Forging Products. Metals, 11(5), 768–768. https://doi.org/10.3390/met11050768

[17] Khodabandeh, A. R., Jahazi, M., Yue, S., & Aghdashi, S. T. (2006). The Determination of Optimum Forging Conditions for the Production of High Strength-High Impact Toughness Automotive Parts. Materials and Manufacturing Processes, 21(1), 105–110. https://doi.org/10.1080/amp-20060666

[18] Sarangi, S. S., Lavakumar, A., Singh, P. K., Katiyar, P. K. & Ray, R. K. (2023). Indentation size effect in steels with different carbon contents and microstructures, Materials Science and Technology, 39(3), 338-346. https://doi.org/10.1080/02670836.2022.2113157

[19] Budiarsa, I. N. (2013). Indentation Size Effect (ISE) of Vickers hardness in steels: correlation with H/E, Applied mechanics and materials, 391, 23-28. https://doi.org/10.4028/www.scientific.net/AMM.391.23

[20] Kozłowska, A., Grajcar, A., Janik, A., Radwański, K., Krupp, U., Matus, K. & Morawiec, M. (2021). Mechanical and thermal stability of retained austenite in plastically deformed bainite-based TRIP-aided mediumMn steels, Archives of Civil and Mechanical Engineering, 21(3), 133. https://doi.org/10.1007/s43452-021-00284-6

[21] De Moor, E., Matlock, D. K., Speer, J. G., & Merwin, M. J. (2011). Austenite stabilization through manganese enrichment. Scripta Materialia, 64(2), 185–188. https://doi.org/10.1016/j.scriptamat.2010.09.040

[22] Jimenez-Melero, E., Van Dijk, N. H., Zhao, L., Sietsma, J., Offerman, S. E., Wright, J. P. & Van der Zwaag, S. (2007). Martensitic transformation of individual grains in low-alloyed TRIP steels, Scripta Materialia, 56(5), 421-424. https://doi.org/10.1016/j.scriptamat.2006.10.041

[23] Shen, Y. F., Qiu, L. N., Sun, X., Zuo, L., Liaw, P. K. & Raabe, D. (2015). Effects of retained austenite volume fraction, morphology, and carbon content on strength and ductility of nanostructured TRIP-assisted steels, Materials Science and Engineering: A, 636, 551-564. https://doi.org/10.1016/j.msea.2015.04.030

[24] Sugimoto, K. I., Misu, M., Kobayashi, M. & Shirasawa, H. (1993). Effects of second phase morphology on retained austenite morphology and tensile properties in a TRIP-aided dual-phase steel sheet, ISIJ international, 33(7), 775-782. https://doi.org/10.2355/isijinternational.33.775

[25] Pereloma, E., Gazder, A. & Timokhina, I. (2016). Retained austenite: transformation-induced plasticity. In R. Colas & G. E. Totten (Eds.), Encyclopedia of Iron, Steel, and Their Alloys (pp. 3088-3103). New York: CRC Press https://doi.org/10.1081/E-EISA-120049200

[26] Xu, M., Yang, Y. G., Chen, J. Y., Tang, D., Jiang, H. T., & Mi, Z. L. (2017). Effects of strain states on stability of retained austenite in medium Mn steels. Journal of Iron and Steel Research International, 24(11), 1125-1130. https://doi.org/10.1016/S1006-706X(17)30163-2

[27] Yamashita, T., Koga, N., & Umezawa, O. (2018). Influence of deformability of retained austenite on martensitic transformation in tension for low alloy steel at low temperatures. ISIJ International, 58(6), 1155-

1161. https://doi.org/10.2355/isijinternational.ISIJINT-2018-033

[28] Timokhina, I. B., Hodgson, P. D., & Pereloma, E. V. (2004). Effect of microstructure on the stability of retained austenite in transformation-induced-plasticity steels. Metallurgical and Materials Transactions A, 35(8), 2331–2341. https://doi.org/10.1007/s11661-006-0213-9

[29] Grajcar, A., Radwański, K., Kilarski, A. & Swadźba, R. (2014) Microstructural Features of Strain-Induced Martensitic Transformation in Medium-Mn Steels with Metastable Retained Austenite. Archives of Metallurgy and Materials, 59(4), 1673–1678, https://doi:10.2478/amm-2014-0283

[30] Bhadeshia, H. K. D. H. (2001) "Bainite in steels: transformation, microstructure and properties." London: IOM, 237-276.

[31] Bhadeshia, H. K. D. H. & Honeycombe, R. W. K. (2017) Steels: microstructure and properties. Butterworth-Heinemann.

[32] Lawrynowicz, Z. (2002). Carbon partitioning during bainite transformation in low alloy steels. Materials Science and Technology, 18(11), 1322-1324.

[33] Porter, D. A., & Easterling, K. E. (2009). Phase transformations in metals and alloys (revised reprint). CRC press.

[34] Ghosh, G., & Olson, G. B. (2001). Computational thermodynamics and the kinetics of martensitic transformation. Journal of Phase Equilibria, 22(3), 199-207.

[35] Jo, H. H., Kim, K. W., Park, H., Moon, J., Kim, Y. W., Shim, H. B., & Lee, C. H. (2023). Estimation of cooling rate of high-strength thick plate steel during water quenching based on a dilatometric experiment. Materials, 16(13), 4792.

[36] Bordereau, V. (2015). Quantitative relationships between chemical composition, microstructure and mechanical properties for bainitic steels (Doctoral dissertation, Ecole Nationale Supérieure des Mines de Paris).

[37] Bhadeshia, H. K. D. H. (2015). Bainite in steels: Theory and practice (3rd ed.). CRC Press.

[38] Christian, J. W., & Mahajan, S. (1995). Deformation-induced phase transformations. Materials Science, 39(1–2), 1–157. https://doi.org/10.1016/0079-6425(94)00002-W

[39] Lee, S. J., Kim, Y. W., & Kim, Y. G. (2006). Effect of prior deformation on austenite grain refinement and phase transformation in steels. Metallurgical and Materials Transactions A, 37A(9), 2859–2867. https://doi.org/10.1007/s11661-006-0118-x